Journal of Engineering Science and Technology
Vol. 15, No. 3 (2020) 1840 - 1854

TILT BASED PASSIVE OPTIMIZATIONS FOR MICROFLUIDICS AND LAB-ON-CHIP DEVICES - A SIMULATION STUDY

Z. E. JEROISH[1,3], K. S. BHUVANESHWARI[1], VIGNESWARAN NARAYANAMURTHY[2, 4,*], R. PREMKUMAR[1], FAHMI SAMSURI[3]

[1]Department of Biomedical Engineering,
Rajalakshmi Engineering College, Chennai 602105, India
[2]Fakulti Teknologi Kejuruteraan Elektrik dan Elektronik
Universiti Teknikal Malaysia Melaka, 76100 Hang Tuah Jaya, Melaka, Malaysia
[3]Faculty of Electrical and Electronics Engineering,
University Malaysia Pahang, Pekan, Pahang 26600, Malaysia
[4]Centre of Excellence for Advanced Research in Fluid Flow,
University Malaysia Pahang, Kuantan 26300, Malaysia
[*]Correspondence: vigneswaran@utem.edu.my

Abstract

Microfluidics-based biochip applications have been increased abruptly in multiple fields because of the advantages in manifolds, which include decreased test sample utilization and reagent consumption with numerous purposes and highly listed benefits. In general, microfluidics involves two different techniques, namely active and passive methods, to enable the fluid flow within the channel that is mounted on the biochip. In this study, we focus on hydrostatic pressure-driven passive pumping methodology as it does not require any external actuators or power source to assist the flow. This technique solely depends on the gravitational pull to enhance fluid flow within the channel. The ultimate aim of this study is to design a microfluidic channel in which the geometrical parameters are optimized, and the respective velocity profile is obtained. The geometrical parameters such as the angle of contact between the channel and the ground (θ), channel dimension, and reservoir dimensions which decide the performance of the microfluidic device. These optimizations in the channels are performed as a theoretical simulation study in 3D modeling software COMSOL Multiphysics 5.0 to analyze the fluid velocity, where θ is varied between 0 degrees and 70 degrees and the channel width (w_c) and channel height (h_c) are varied between 1 mm to 10 mm and 0.05 mm to 0.5 mm, respectively. Also, the reservoir diameter (d_r) and reservoir height (h_r) are varied between 6 mm and 10 mm, and 0.5 mm and 3 mm, respectively for analyzing the velocity profiles. From the obtained results, it is observed that the overall flow velocity ranges between 7.27×10^{-5} – 3.77870×10^{-2} m/s. Hence an individual can select the best optimizations of the geometrical parameters and their respective velocity for designing a microfluidic chip with specific applications upon following this article.

Keywords: Hydrostatic pressure-driven, Microfluidics, Optimization, Passive pumping.

1. Introduction

Microfluidics is a well-known multidisciplinary field that incorporates various fields, namely Engineering, Physics, Chemistry, Biochemistry, and Nanotechnology that has been emerged in the early 1980s and utilized for the development of DNA chips, and Lab-On-Chip (LOC) technology [1, 2]. Microfluidics deals with the control and manipulation of the fluids and enables mass transport of the fluids that processes only a low volume of fluids to achieve high throughput screening with high efficiency and low energy consumption. Biochips are miniaturized laboratories that grant many tests to be taken part simultaneously to gain high throughput and speed, whereas the digital biochip is the microfluidic array filled with the adjacent cells that are most commonly used in biomedical fields [3-5]. More often, the surface area of the biochip does not exceed the size of the fingernail. However, millions of mathematical operations can be performed within seconds with high efficiency and throughput. Similarly, LOC is an integrated device that involves one or several laboratory functions in a single integrated circuit whose size is about millimeter or centimeter with low fluid handling potential. Recent advancements in microfluidics include the development of Molecular biology procedures for enzymatic analysis and proteomics. In addition to this, the emerging application of microfluidics consists of the Point-Of-Care diagnosis of diseases [6, 7]. Also, microfluidics devices possess the ability of continuous sampling and real-time testing of samples and pathogens. An immense benefit is widely observed in personalized medicine, early diagnostics, and drug patenting fields.

1.1. Hydrostatic pressure-driven passive microfluidics

Broadly microfluidic devices can be categorized into actively driven microfluidic devices and passively driven microfluidic devices. Passively driven microfluidics is defined as the techniques which do not rely on any external supporting devices to facilitate fluid flow within the channel. Instead, it is solely based on fluid properties and channel parameters [8, 9]. One such passively driven technique is hydrostatic pressure-driven flow, where the pressure exerted by a fluid due to the effect of gravity that facilitates the fluid flow. The hydrostatic pressure increases proportionally to the depth when measured from the surface. This is because of the increasing weight of the fluid that exerts the downward force from above to assist the fluid flow within the channel. From the numerous articles available, we represented a few handpicked articles that deal with the passive driven microfluidics.

In 2005, Rettig and Folch et al. established an optimization study that had incorporated high cell occupancies and also paved the way to uplift the single-cell occupancies upon varying the microwell diameter and its depth [10]. In 2009, Park et al. demonstrated that the geometry of the wells could also cause deviation in the flow pattern and decrease the trapping ability. Hence the microwell dimension is optimized for attaining efficient cell trapping [11]. Vangelooven et al. described the optimizations in the gap width and the axial length of the distributor to generate a steady transversal flow within the microfluidic channels [12]. In 2013, Karimi et al. reported an overview which had imparted about the cell/particle sorting techniques using hydrodynamic effects to assist the fluid flow in microchannels [13]. In addition to this, Zografos et al. had studied the effects of optimization on the channel length and depth to achieve constant strain-rates in the viscoelastic

fluids [14]. In 2017, Jasper James et al. had proposed an idea to develop a biochip for Single Cell Analysis (SCA) in microfluidics using a vertical trapping array that involved the hydrodynamic based cell trapping that relied on the surface topographies. It also provided a comparative analysis of the multiple designs that can effectively capture the single cell [15].

In 2018, Vigneswaran Narayanaumurthy et al. had proposed an article which had described the effects of fluid channel design and microwell array design for single-cell trapping efficiency that employed the use of Pipette Petri dish Single-Cell Trapping (PP-SCT) technique that is capable of vertical cell trapping. The trapping efficiency was analyzed in three designs, namely straight channel, branched channel, and serpent-shaped channel. It was observed that the serpent channel had better single-cell trapping efficiencies [16, 17]. Thus, in this analysis serpent channel design is considered for further studies.

To the best of our knowledge, none of the studies from the literature survey had investigated the efficiency of hydrostatic-based fluid channel designs upon optimizing the tilt angle, the reservoir, and the channel dimensions. This study is an extension of the work carried out in [16]. In this paper, we have further analyzed the various parameters and features for deriving the optimal conditions through the numerical approach. We want to impart a clear idea on varying velocity profile concerning the changes in the various parameters of the channel and the reservoirs, which utilizes the gravity-based passive flow. By analyzing the velocity profile of various optimizations in the channels, one can use these specified parameters for attaining the desired velocity. Finally, we also concluded the optimum parameters for obtaining maximum velocity within the specified channel dimensions that can suit well within the glass slide of the standard size. Also performed the analysis of velocity profile that has been obtained as a result of the various optimizations performed in the channel that helps in selecting a suitable optimization parameter to gain a better flow. These offer a wide range of applications in research and development works for attaining specific velocities.

2. Methods

New methods and various execution platforms in the field of passive flow microfluidics that helps in designing a high throughput device with less expertise and complexity, to analyze the velocity for various applications.

2.1. Device design

In this study, the device dimension is based on the previous review [16]. In the work as mentioned above, the device design was made of 3 inches × 1 inch in size, and standard Petri dishes of dimensions 90 mm × 15 mm (Sigma, St Louis, MO, USA) were examined. Petri dishes have a lower dish (LD) and an upper dish (UD) of dimensions 87 mm × 15 mm and 90 mm × 7 mm respectively. With these standard dimensions, this simulation study is performed. Along the sidewall of the petri dish, the inlet side of the biochip is made to lean upon it, and the outlet side is placed inside the petri dish base along its diameter. Then the sample is placed at the inlet well, which flows through the channel as a result of the generated pressure due to gravity and gets collected at the outlet well. During the extreme operational condition, one can use sticky tape to lock down the position of the biochip with the petri dish. The fluid flowing through the channel is calculated by using the formula;

Fluid flow rate = Area of the channel × Velocity of the liquid, which can also be mentioned as in Eq. (1),

$$Q = AV \tag{1}$$

where Q is the liquid flow rate (m^3/s), A is the cross-sectional area of the channel (m^2), and V is the velocity of the liquid (m/s). Device design in the simulation study is computed with the no-slip boundary condition where the velocity of the fluid is almost 0 near the walls, and it gradually increases as we move towards the center of the flow path.

The inlet pressure values can be calculated with the Eq. (2) namely,

$$p = \rho g h \tag{2}$$

where, p is pressure in the fluid sample (Pa), ρ is the density of the liquid (kg/m^3), g is the acceleration of gravity (m/s^2), and h is the height of the fluid column or depth in the fluid (μm) from the ground.

The height of the fluid column varies concerning the varying angle of contact of the channel. In microenvironments predominantly, the laminar flow pattern is seen, since the viscous forces dominate inertial forces. This can be determined by the Reynolds number (Re). The laminar flow pattern is observed when the Reynolds number is less than 2300. Reynolds number can be calculated using the relation given in Eq. (3);

$$\text{Re} = \frac{\text{Inertial Force}}{\text{Viscous Force}} \tag{3}$$

In this work, incompressible flow is considered since the fluids with a constant density (ρ) are incompressible. Their flow along the channel is governed by the Navier-Stokes equation, Bernoulli equation, Hagen Poiseuille equation, and the Continuity Equation. The flow material considered in this work is water. The properties of the studied materials are given in Table 1.

Table 1. Material and its properties used in the study.

Components	Property	Value
Fluid (water)	Dynamic Viscosity (μ)	8.90×10^{-4} (Pa/s)
	Density (ρ)	1000 (kg/m^3)
Channel	Channel Surface Roughness	Glass (0.0015 mm)
Pressure	Inlet	$\rho g h$

2.2. Mesh optimisation

The microfluidic simulation analysis in COMSOL requires appropriate meshing for every model. Meshing is essential for Finite Element Analysis (FEA). In COMSOL Multiphysics, the range of meshing element size varies from extremely fine to extremely coarse. Upon customizing the meshing sequence, the memory requirements can be controlled, which results in efficient and accurate simulation [18]. In this study, the physics-controlled mesh for fluid flow is used, as shown in Fig. 1. To determine the appropriate meshing for the study, we have run the initial simulation on the extremely coarser mesh, and then successive simulations were computed with progressively smaller meshes until the maximum velocity is obtained. From the obtained velocity profiles for each type of mesh, the best of all computations are taken for further optimizations. Too coarse a mesh will result in

limited data points. Moreover, distorted elements are created due to improper meshing can affect the geometric and numerical representation of the model. Both result in reduced accuracy. Hence finer the mesh produces the best result with accurate calculations.

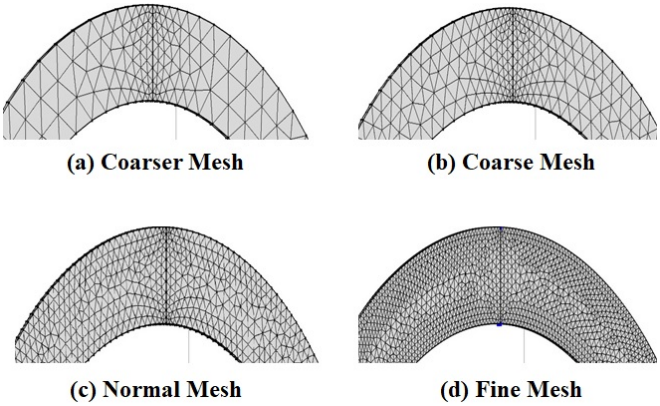

Fig. 1. Interior view of different types of mesh applied in the channel geometry.

Figure 2 shows the graphical plots of gradually increasing velocity profiles in various types of applied mesh. Gradually increasing velocity is obtained at the fine mesh level during the simulation process. From the simulation results, it can be stated that the minimum element quality computed at the tilt angle of 40 degrees is 0.01278, and the number of edge elements calculated is about 3178 with 54 vertex elements. This stands as the detailed element analysis on comparing with all the other kinds of meshes. Therefore, fine mesh is employed for further computations.

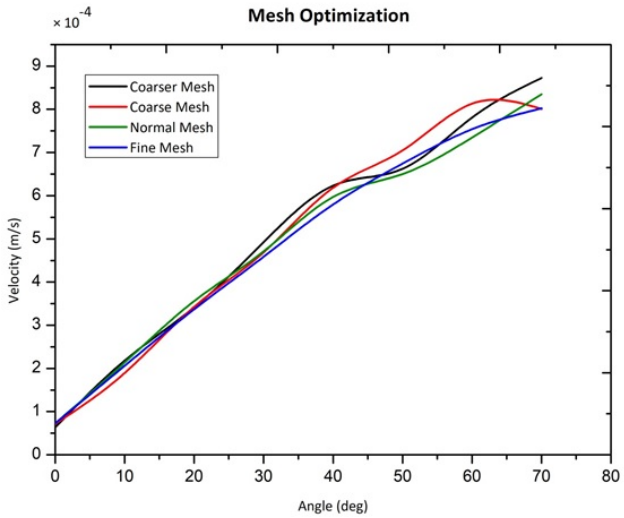

Fig. 2. Graphical plot shows the velocity profile for various types of applied mesh.

3. Results and Discussion

In order to design the passive flow microfluidic device with maximum efficiency, the results obtained from the following optimization factors could be considered for better development of the device.

3.1. Optimization factors

From the previous studies, as noted in the literature survey, the velocity profiles are extracted from the channel with a different set of optimization factors [18]. Figure 3 represents the possible optimizations that could be made in the device parameters to attain a better velocity profile, and also to end up with a better design. Based on the comparative study made, the Upper Dish (UD) of the petri dish is taken to achieve the high results where the gravity-driven flow can be accomplished with ease [19]. It is found that the parameters of inlet reservoir have high impact concerning these varying parameters, so the parameters of outlet reservoir are maintained constant as in Fig. 3 as it does not have. It is observed that the yield at the input reservoir side has produced a satisfying output with a superior-velocity profile when evaluated with the outlet reservoir side.

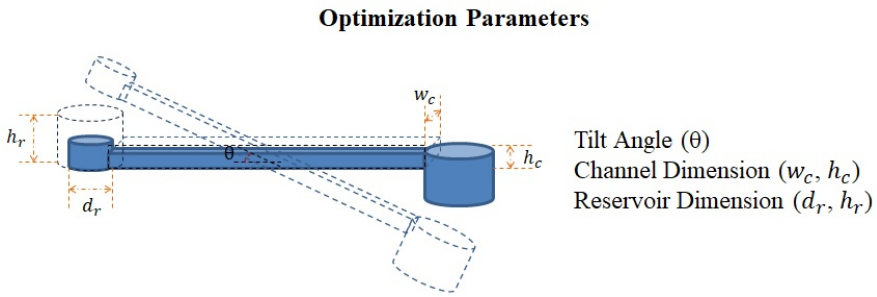

Fig. 3. 2-Dimensional view of the various optimization factors.

3.2. Tilt angle

The angle of contact of the biochip along the surface of the petri dish is adjusted in such a way that the flow is governed from the steep input side towards the output side where the gravity pulls down the fluid into the microfluidic channel. On adjusting the tilt angle (θ), the velocities fluctuate due to the varying height from their previous positions. To obtain a better flow rate, the study is carried out for a range of θ values where the pressure difference between two ends (inlet and outlet reservoir) is assessed through the Bernoulli's formula. The product of a gravitational constant (g), fluid density (ρ), and height (h) of the inlet reservoir from the surface of UD is calculated for every θ. The velocity profile is obtained for different θ with the constant w_c of 2000 µm and h_c of 200 µm. The d_r is retained at 3000 µm and h_r of 2000 µm.

Figure 4 shows the simulation results of angle optimization. (a) the channel geometry with the minimum angle optimization of 0 degrees is shown in the 3D view, (b) depicts the simulation results for the designed channel along with the velocity profile that has been acquired, (c) shows the 2D cut plane along the YZ axis of the channel geometry which helps in the velocity profile analysis, (d) shows

the channel geometry with the maximum angle optimization of 70 degrees in the 3D view, (e) depicts the simulation results for the designed channel along with the velocity profile that has been acquired, (f) shows the 2D cut plane along the YZ axis of the channel geometry which helps in the velocity profile analysis.

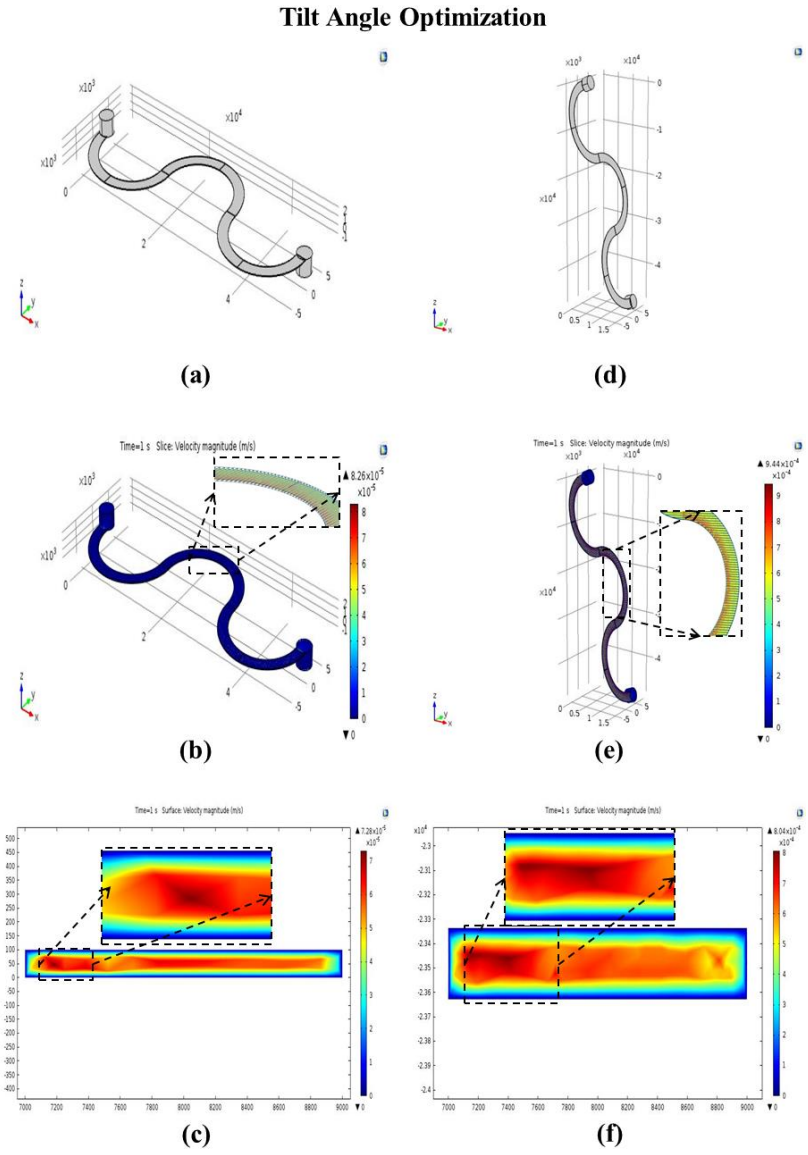

Fig. 4. Simulation images of angle optimization.

Figure 5 indicates the velocity profile of the fluid that is obtained during angle optimization. It can be concluded that the velocity profile of the fluid flowing through the fluid column has increased persistently. The maximum velocity obtained is 8.0237×10^{-4} m/s at the θ value of 70 degrees, and the minimum velocity 7.27×10^{-5} m/s is noted at the θ value of 0 degree where there is no elevation.

Henceforth it can be understood that greater the θ greater the gravitational force exists between them to pull the fluid into the column to obtain an increased velocity profile. Since this study is an extension work of [16] where they have clearly mentioned that better optimization can occur between 15 and 40 degrees, so we have choosen θ of 40 degrees for further optimizations. In addition to that sample loading and passive flow mechanism faces some intricacies when the θ is beyond 70 degrees. Therefore the θ optimizations are performed only within the range of 0 and 70 degrees.

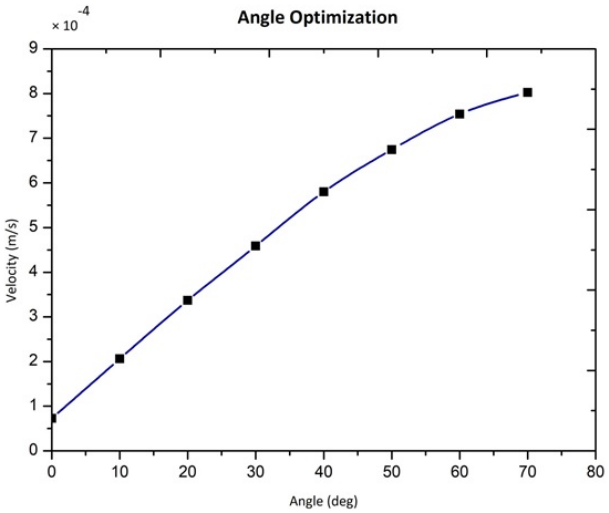

Fig. 5. Graphical plot shows the relationship between the tilt angle and the acquired velocity profile.

3.3. The dimension of the channel

Along the length of the channel, that is, at the sides, friction is created as the fluid flows against the edges. Fluids flowing through a wide, deep channel encounter less resistance than the fluid flowing in a narrow, shallow channel since a smaller proportion of the total fluid molecules will be slowed by the channel edges, and hence, the center of the channel experiences the most significant velocity.

With the θ value of 40 degrees, the channel is inspected by varying h_c from 50 µm to 500 µm, and w_c from 1000 µm to 10000 µm. If w_c is 1000 µm and 2000 µm, then d_r and h_r is fixed as 3000 µm and 2000 µm respectively. However, d_r cannot be kept stable as the increase in the w_c does not settle with the stable d_r. Hence, the d_r is again altered to 10000 µm for the w_c of 5000 µm and 10000 µm. Therefore, finalizing proper channel length plays an essential role in maintaining the channel geometry. This length of the channel is measured in such a way that it fits into the biochip within the given dimensions upon fabrication.

Figure 6 shows the simulation results procured during the channel optimization. (a) the w_c 1000 µm and h_c 50 µm with the optimized θ of 40 degrees has been designed and shown in the 3D view, (b) depicts the simulation results for the designed channel along with the velocity profile that has been acquired, (c) shows the 2D cut plane along the YZ axis of the channel geometry which helps in

the velocity profile analysis, (d) the w_c 10000 µm and h_c 50 µm with the optimized θ of 40 degrees has been designed and shown in the 3D view, (e) depicts the simulation results for the designed channel along with the velocity profile that has been acquired, (f) illustrates the 2D cut plane along the YZ axis of the channel geometry which helps in the velocity profile analysis.

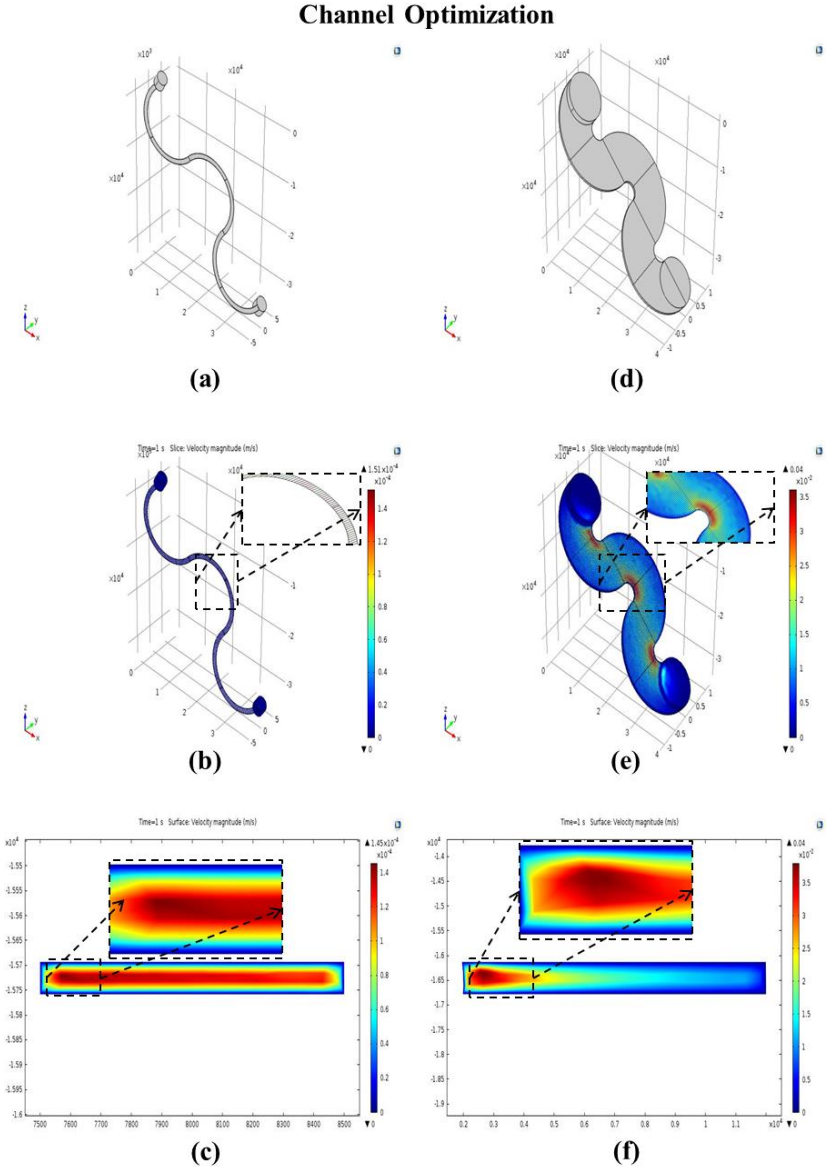

Fig. 6. Simulation images of channel optimization.

The graph in Fig. 7 imparts a clear idea on the velocity profile and its relation with the channel geometry, which includes the width and height of the channel. The channel optimization results in the maximum velocity of 0.0377 m/s at the w_c

10000µm and h_c 500µm. From the computational analysis, it is noted that the velocity profile increased exponentially within the considered w_c and h_c. Therefore, further simulation study and analysis are progressed with the w_c and h_c of 5000 µm and 200 µm respectively, since it possesses the medium velocity.

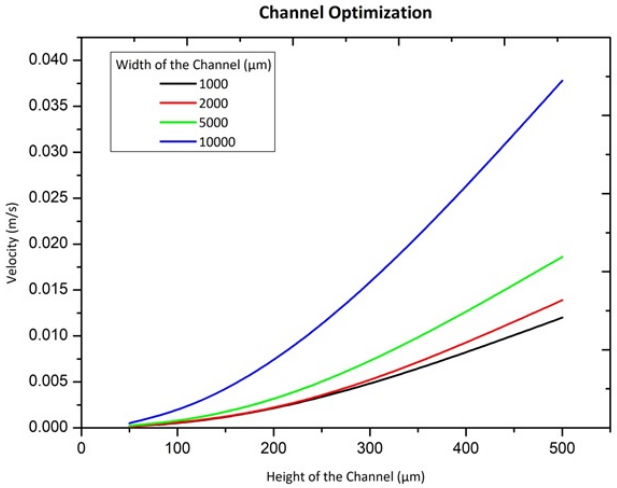

Fig. 7. Graphical plot showing the relationship between w_c, h_c, and velocity profile.

3.4. Reservoir dimension

The h_r and d_r constitute the entire pressure of the fluid, which plays a vital role in fluid flow, where smaller the h_r and d_r, lesser the gravity exists between the reservoir and the surface to drive the fluid into the channel. Hence, h_r and d_r are optimized for a specific range to obtain a better velocity profile. As the height varies, change in the velocity is spotted. The θ of 40 degrees, and the w_c and h_c of 5000 µm and 200 µm respectively are maintained as the pre-set parameters, only the d_r and h_r of the inlet and outlet reservoir are varied. In which, the h_r of the inlet and the outlet reservoir is modified between 500 µm and 3000 µm. Similarly, d_r is varied between 6000 µm and 10000 µm.

Figure 8 shows the simulation results found during reservoir optimization. (a) the channel with the optimized θ of 40 degrees, w_c of 5000 µm, h_c of 200 µm, h_r of 500 µm and d_r of 6000 µm has been designed and shown in the 3D view, (b) depicts the simulation results for the designed channel along with the velocity profile that has been acquired, (c) shows the 2D cut plane along the YZ axis of the channel geometry which helps in the velocity profile analysis; (d) the channel with the optimized θ of 40 degrees, w_c of 5000 µm, h_c of 200 µm, h_r of 3000 µm and the d_r of 10000 µm has been designed and shown in the 3D view, (e) depicts the simulation results for the designed channel along with the velocity profile that has been acquired, (f) shows the 2D cut plane along the YZ axis of the channel geometry which helps in the velocity profile analysis.

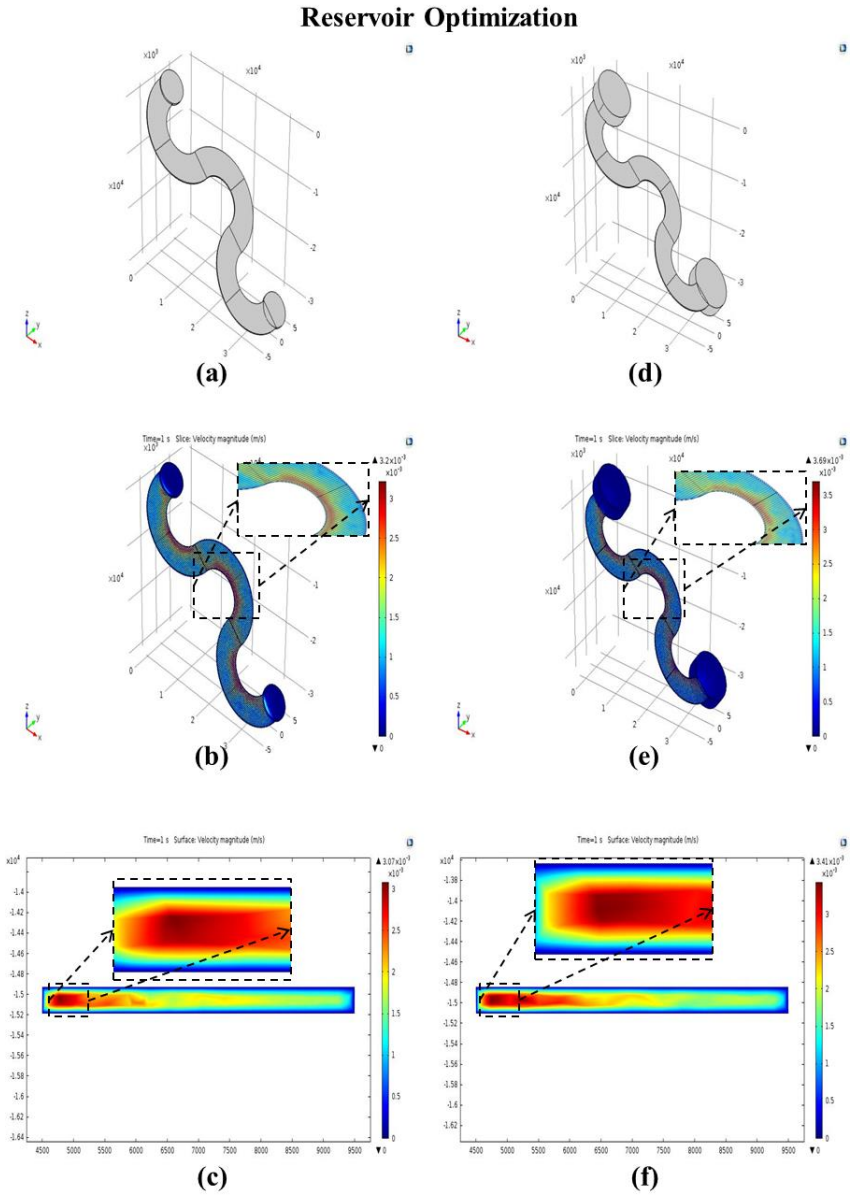

Fig. 8. Simulation images of reservoir optimization.

Figure 9 represents the velocity profile variation acquired in reservoir optimization. Reservoir with the d_r of 6000 µm and h_r of 3000 µm produced the maximum velocity of 3.5×10^{-3} m/s. From this, it is concluded that the velocity profile obtained during the optimization in h_r and d_r does not increase continually. However, when the d_r is merely equal to the w_c, the variation in velocity increases gradually. Beside all these things, the d_r is inversely proportional to the velocity. Hence the selection of d_r is essential to obtain a better velocity for specific applications.

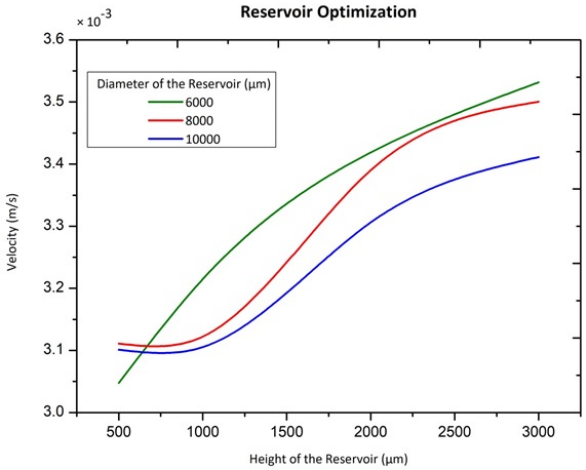

Fig. 9. Graphical plot showing the velocity profile for varying d_r and h_r.

3.5. Velocity profile analysis

From the study, the velocities of various optimizations are analyzed and characterized into three different sections as high, medium, and low velocity, as shown in Fig. 10. These classifications help to find out the distinct parameters of the device to achieve a specific velocity profile under certain applications. From the graph, it is evident that the channel parameters can bring about a noticeable change in velocity; hence, it is involved in designing the high-velocity devices. For instance, the w_c of 2000 µm and 5000 µm with 500 µm h_c has an average velocity. Whereas the w_c of 10000 µm with the same h_c employs the high velocity. However, the angle and the reservoir parameters are studied when there is a requirement for minor changes in the velocity.

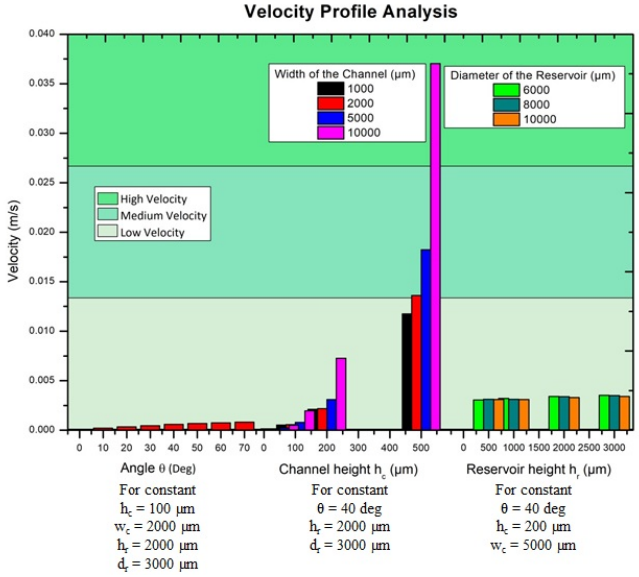

Fig. 10. Bar graph signifying the velocity profile in the distinct regions.

4. Conclusion and Future Perspectives

Microfluidics is established on a vast scale since its introduction in the field of biological and medical applications. The extended reach of microfluidics has been declined by various factors. One such factor is to design an automated and recurring function microfluidic device is to exclude the external equipment. An additional issue is mass production; presently, distinct applications require various designs. Hence, limiting the general fabrication of one type of device that will suit every purpose is a tedious task. The multidisciplinary nature of microfluidics demands for the continuous coordination between different fields, to reach its full potentials. A persistent growth and significant expansion beyond simple proof-of-concept systems into the extensive real-world and commercial applications are expected. The function of passive flow microfluidics had eliminated these consequences.

In this study, passive flow microfluidics is highly concentrated due to its advantages that stand as the successor of these techniques in numerous fields. As it depends on the fluid properties, it is more convenient and cost-efficient. The gravity existing between the channel geometry and the surface allows the fluid to flow within the column. The velocity is acquired in the range of 7.27×10^{-5} – 8.0237×10^{-4} m/s when the θ is maintained between 0 degrees and 70 degrees. Along with the θ, channel parameters, such as h_c and w_c are also varied from 0.05 mm to 0.5 mm and 1 mm to 10 mm for which the flow velocity is found to be 1.44×10^{-4} to 0.0377 m/s. The reservoir dimensions, such as d_r and h_r are altered between 6 mm and 10 mm, and between 0.5 mm and 3 mm respectively, together with the channel and angle optimization parameters, to get precise velocity, which falls under the range of 3.04×10^{-3} and 3.5×10^{-3} m/s. Therefore, it is concluded that the selection of proper mesh factors, tilt angle, channel, and reservoir parameters play a crucial role in achieving laminar flow.

Hence, proper designing and simulation have to be performed for accurate results. This work can be extended into a fabrication analysis study since the entire study is carried out in the simulation software, and also researchers can consider working on the low and high-velocity profile since the medium velocity is alone analyzed in this work.

Acknowledgements

Authors would like to thank the support from Universiti Teknikal Malaysia Melaka, BME Dept. Rajalakshmi Engineering College, University Malaysia Pahang and acknowledge the research grant RDU190108.

Nomenclatures

A	Cross-sectional area of the channel, m^2
d_r	Diameter of the reservoir, µm
G	Acceleration of gravity, m/s^2
H	Height of the fluid column, µm
h_c	Height of the channel, mm
h_r	Height of the reservoir, µm
P	Pressure in the fluid sample, Pa
Q	Liquid flow rate, m^3/s

Re	Reynolds number
V	Velocity of the liquid, m/s
w_c	Width of the channel, mm

Greek Symbols

ρ	Density of the liquid, kg/m^3
θ	Angle of contact between the channel and the ground, deg.
μ	Dynamic Viscosity, Pa/s

Abbreviations

FEA	Finite Element Analysis
LD	Lower Dish
LOC	Lab-On-Chip
PP-SCT	Pipette Petri dish-Single Cell Trapping
SCA	Single Cell Analysis
UD	Upper Dish

References

1. Webster, A.; Greenman, J.; and Haswell, S.J. (2011). Development of microfluidic devices for biomedical and clinical application. *Journal of Chemical Technology & Biotechnology*, 86(1), 10-17.
2. Gao, Z.; Ng, K.; Furlani, E.; Chwalek, J.; and Hawkins, G. (2010). MEMS-based microfluidic devices. *International Conference on Nanochannels, Microchannels, and Minichannels*. Montreal, Canada, 863-868.
3. Su, F.; and Chakrabarty, K. (2008). High-level synthesis of digital microfluidic biochips. *ACM Journal on Emerging Technologies in Computing Systems*, 3(4), 1-32.
4. Chakrabarty, K.; Fair, R.B.; and Zeng, J. (2010). Design Tools for digital microfluidic biochips: toward functional diversification and more than moore. *IEEE Transactions on Computer-Aided Design of Integrated Circuits and Systems*, 29(7), 1001-1017.
5. Millington, D.S.; Sista, R.; Eckhardt, A.; Rouse, J.; Bali, D.; Goldberg, R.; Cotten, M.; Buckley, R.; and Pamula, V. (2010). Digital microfluidics: a future technology in the newborn screening laboratory? *Seminars in Perinatology*, 34(2), 163-9.
6. Volpatti, L.R.; and Yetisen, A.K. (2014). Commercialization of microfluidic devices. *Trends Biotechnol*, 32(7), 347-50.
7. Whitesides, G.M. (2006). The origins and the future of microfluidics. *Nature*, 442(7101), 368-73.
8. Stone, H.A.; Stroock, A.D.; and Ajdari, A. (2004). Engineering Flows in small devices. *Annual Review of Fluid Mechanics*, 36(1), 381-411.
9. Sackmann, E.K.; Fulton, A.L.; and Beebe, D.J. (2014). The present and future role of microfluidics in biomedical research. *Nature*, 507(7491), 181-189.
10. Rettig, J.R.; and Folch, A. (2005). Large-scale single-cell trapping and imaging using microwell arrays. *Analytical Chemestry*, 77(17), 5628-34.
11. Park, J.Y.; Morgan, M.; Sachs, A.N.; Samorezov, J.; Teller, R.; Shen, Y.; Pienta, K.J.; and Takayama, S. (2010). Single cell trapping in larger microwells

capable of supporting cell spreading and proliferation. *Microfluid Nanofluidics*, 8(2), 263-268.

12. Vangelooven, J.; and Desmet, G. (2010). Computer aided design optimisation of microfluidic flow distributors. *Journal of Chromatography A*, 1217(43), 6724-6732.
13. Karimi, A.; Yazdi, S.; and Ardekani, A.M. (2013). Hydrodynamic mechanisms of cell and particle trapping in microfluidics. *Biomicrofluidics*, 7(2), 21501.
14. Zografos, K.; Pimenta, F.; Alves, M.A.; and Oliveira, M.S. (2016). Microfluidic converging/diverging channels optimised for homogeneous extensional deformation. *Biomicrofluidics*, 10(4), 043508.
15. James, J.; Sushmitha, M.; Premkumar, R.; Narayanamurthy, V.; and Kalpana, R. (2017). Microfluidic micro-well (size and shape) by numerical optimization for single cell applications: Vertical trapping approach, *2017 International conference on Microelectronic Devices, Circuits and Systems (ICMDCS)*. Vellore, India, 1-6.
16. Narayanamurthy, V.; Lee, T.; Firus Khan, A.Y.; Samsuri, F.; Mohamed, K.; Hamzah, H.; and Baharom, M. (2018). Pipette petri dish single-cell trapping (PP-SCT) in Microfluidic platforms: A Passive hydrodynamic technique. *Fluids*, 3(3), 51.
17. Narayanamurthy, V.; Nagarajan, S.; Firus Khan, A.Y.; Samsuri, F.; and Sridhar, T.M. (2017). Microfluidic hydrodynamic trapping for single cell analysis: mechanisms, methods and applications. *Analytical Methods*, 9(25), 3751-3772.
18. Qiu, X.; Huang, J.H.; Westerhof, T.M.; Lombardo, J.A.; Henrikson, K.M.; Pennell, M.; Pourfard, P.P.; Nelson, E.L.; Nath, P.; and Haun, J.B. (2018). Microfluidic channel optimization to improve hydrodynamic dissociation of cell aggregates and tissue. *Scientific Reports*, 8(1), 2774.
19. Nedelcu, O.T.; and Stanciu, I. (2012). Optimization of a passive micromixer using models based on variable diffusion coefficient, *CAS 2012 (International Semiconductor Conference)*. Sinaia, Romania, 411-414.